Supplementary material to "Mapping the dependence of BC radiative forcing on emission region and season"

Petri Räisänen[1], Joonas Merikanto[1], Risto Makkonen[1,2], Mikko Savolahti[3], Alf Kirkevåg[4], Maria Sand[5], Øyvind Seland[4], and Antti-Ilari Partanen[1]

[1]Finnish Meteorological Institute, Climate Research, Helsinki, Finland
[2]University of Helsinki, Institute for Atmospheric and Earth System Research, Helsinki, Finland
[3]Finnish Environment Institute, Climate and Air Pollution, Helsinki, Finland
[4]Norwegian Meteorological Institute, Oslo, Norway
[5]CICERO Center for International Climate Research, Oslo, Norway

Correspondence: Petri Räisänen (petri.raisanen@fmi.fi)

This Supplementary material contains eight figures. Figures S1–S5 are related to Sect. 4.2 of the main paper (additivity and linearity of BC radiative forcings). Correspondingly, Figs. S6–S8 are related to the impact of emission season on BC radiative forcing, discussed in Sect. 5.3 of the main paper.

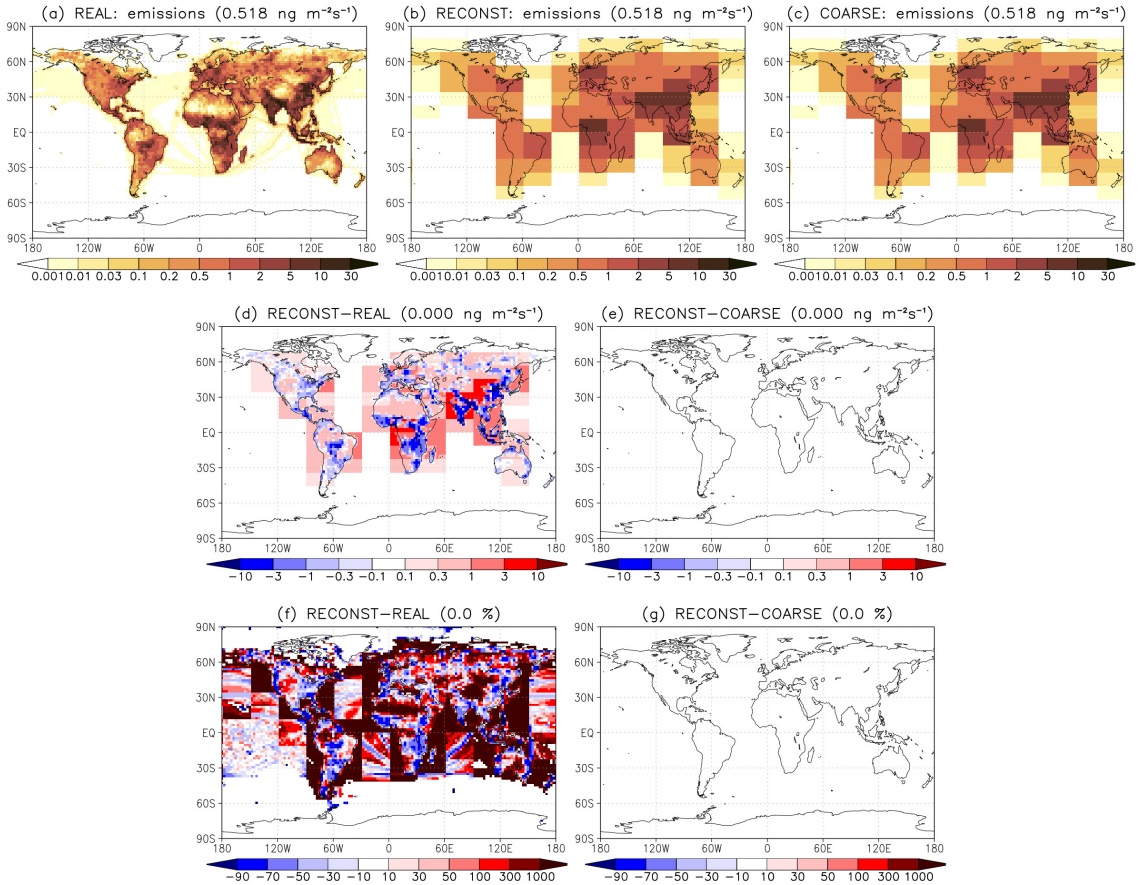

Figure S1. BC emissions (in units of $\mathrm{ng\,m^{-2}\,s^{-1}} = 10^{-12}\,\mathrm{kg\,m^{-2}\,s^{-1}}$) in the experiments (a) REAL and (c) COARSE. Between them, (b) shows the emissions reconstructed for REAL using Eq. (3) in the main paper. The reconstruction for COARSE is virtually identical (not shown). (d) and (e): Reconstruction errors ($\mathrm{ng\,m^{-2}\,s^{-1}}$). (f) and (g): Relative reconstruction errors (%). Global-mean values are indicated in the panel titles.

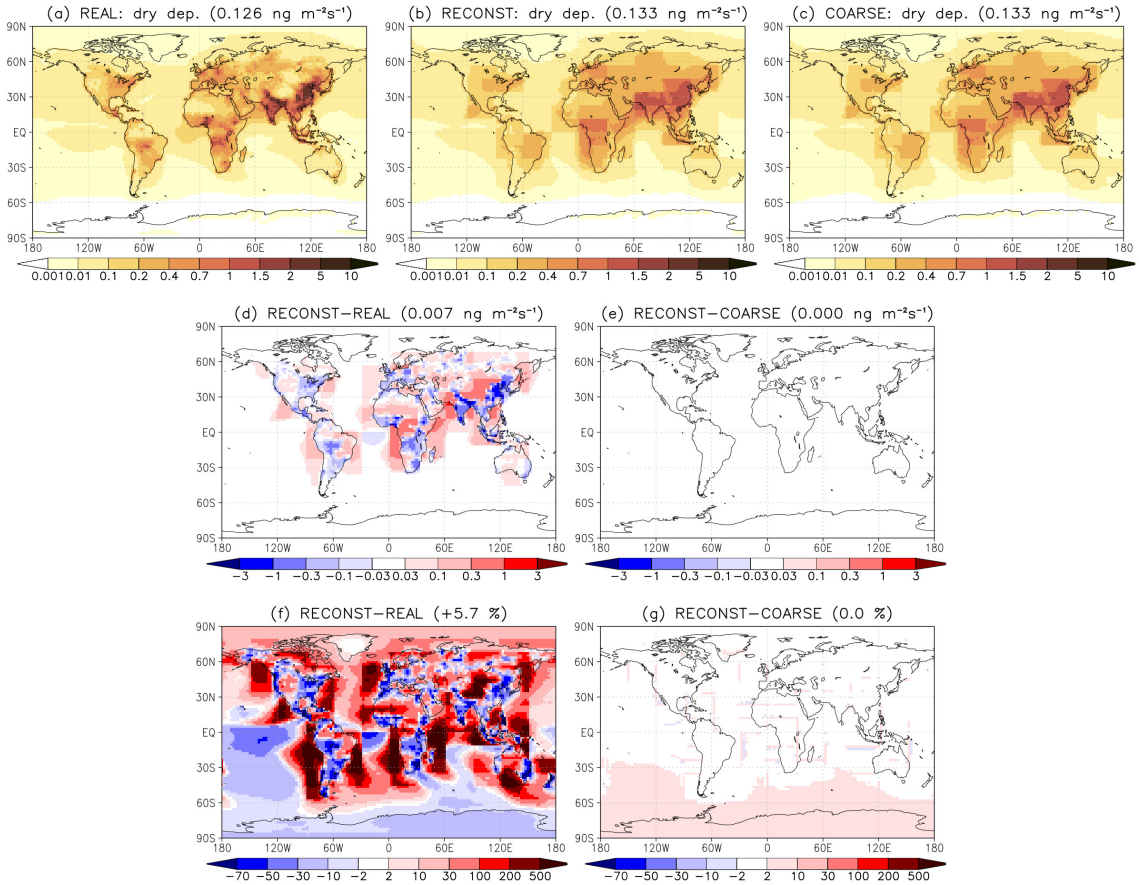

Figure S2. BC dry deposition rate (in units of $\mathrm{ng\,m^{-2}\,s^{-1}} = 10^{-12}\,\mathrm{kg\,m^{-2}\,s^{-1}}$) in the experiments (a) REAL and (c) COARSE. Between them, (b) shows the dry deposition rate reconstructed for REAL using Eq. (3) in the main paper. The reconstruction for COARSE is virtually identical (not shown). (d) and (e): Reconstruction errors ($\mathrm{ng\,m^{-2}\,s^{-1}}$). (f) and (g): Relative reconstruction errors (%). Global-mean values are indicated in the panel titles.

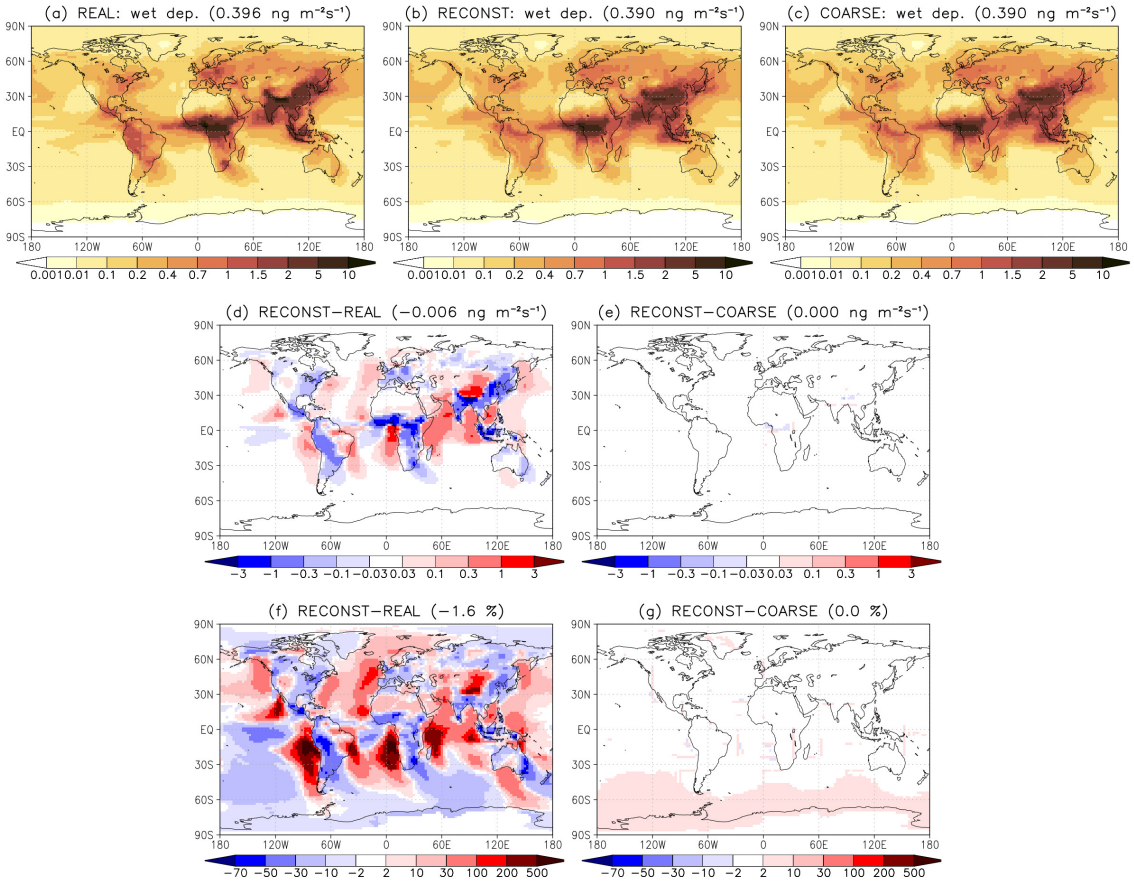

Figure S3. BC wet deposition rate (in units of $\mathrm{ng\,m^{-2}\,s^{-1}} = 10^{-12}\,\mathrm{kg\,m^{-2}\,s^{-1}}$) in the experiments (a) REAL and (c) COARSE. Between them, (b) shows the wet deposition rate reconstructed for REAL using Eq. (3) in the main paper. The reconstruction for COARSE is virtually identical (not shown). (d) and (e): Reconstruction errors ($\mathrm{ng\,m^{-2}\,s^{-1}}$). (f) and (g): Relative reconstruction errors (%). Global-mean values are indicated in the panel titles.

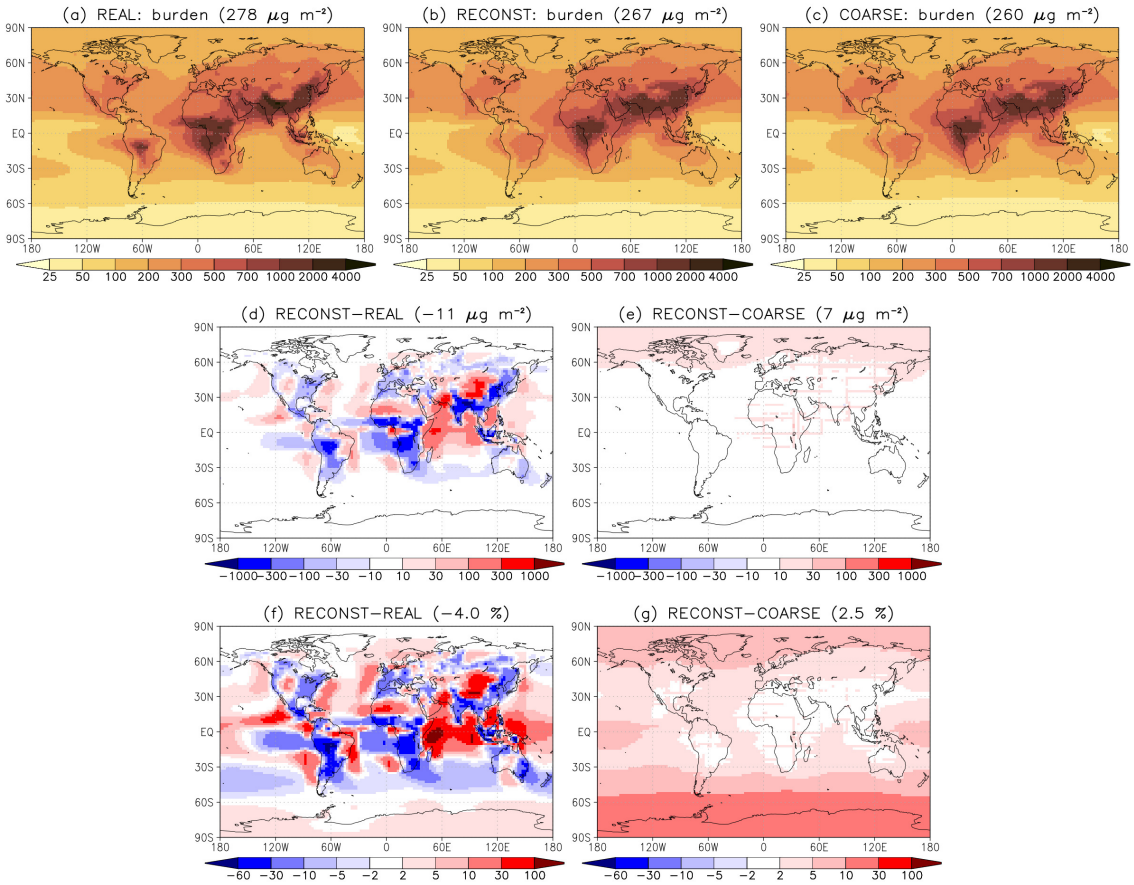

Figure S4. BC burden (in units of $\mu g\,m^{-2} = 10^{-9}\,kg\,m^{-2}$) in the experiments (a) REAL and (c) COARSE. Between them, (b) shows the BC burden reconstructed for REAL using Eq. (3) in the main paper. The reconstruction for COARSE is virtually identical (not shown). (d) and (e): Reconstruction errors ($\mu g\,m^{-2}$). (f) and (g): Relative reconstruction errors (%). Global-mean values are indicated in the panel titles.

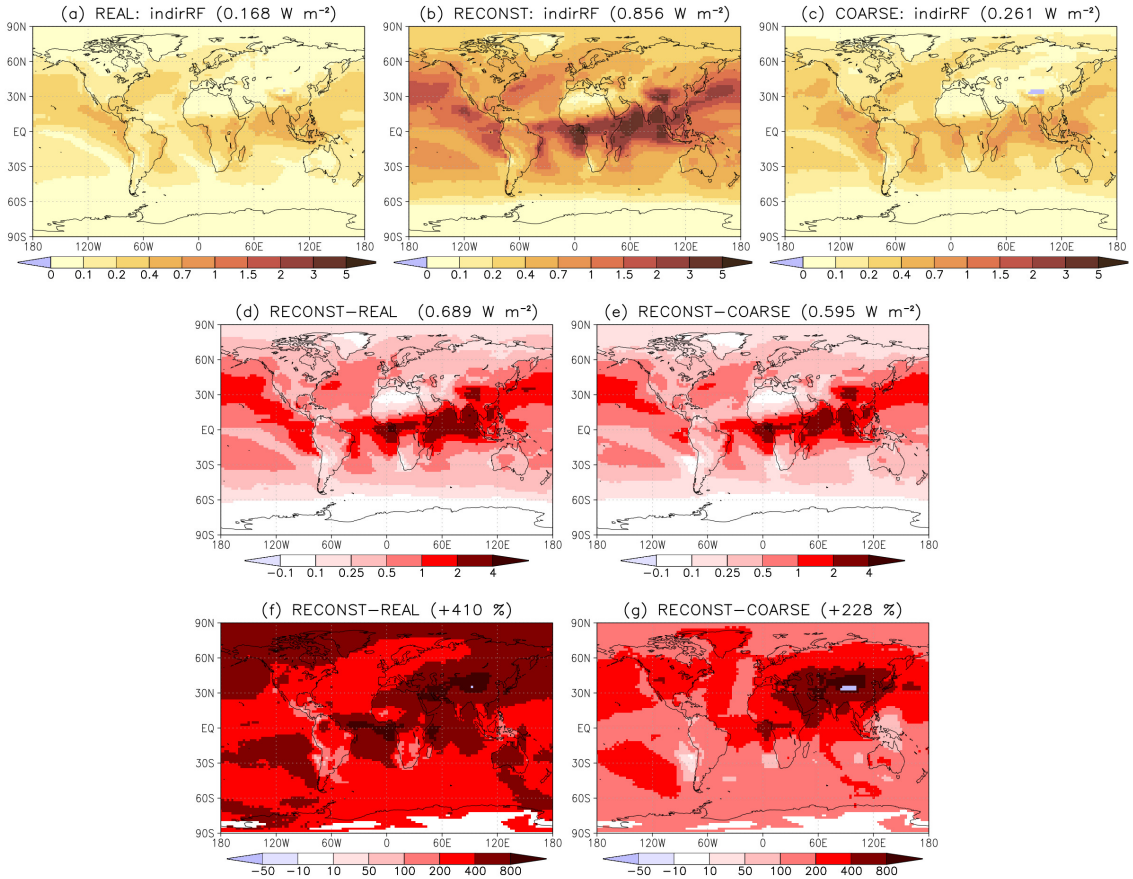

Figure S5. BC indirect radiative forcing at TOA ($\mathrm{W\,m^{-2}}$) in the experiments (a) REAL and (c) COARSE. Between them, (b) shows indirRF reconstructed for REAL using Eq. (3) in the main paper. The reconstruction for COARSE is virtually identical (not shown). (d) and (e): Reconstruction errors ($\mathrm{W\,m^{-2}}$). (f) and (g): Relative reconstruction errors ($\%$). Global-mean values are indicated in the panel titles.

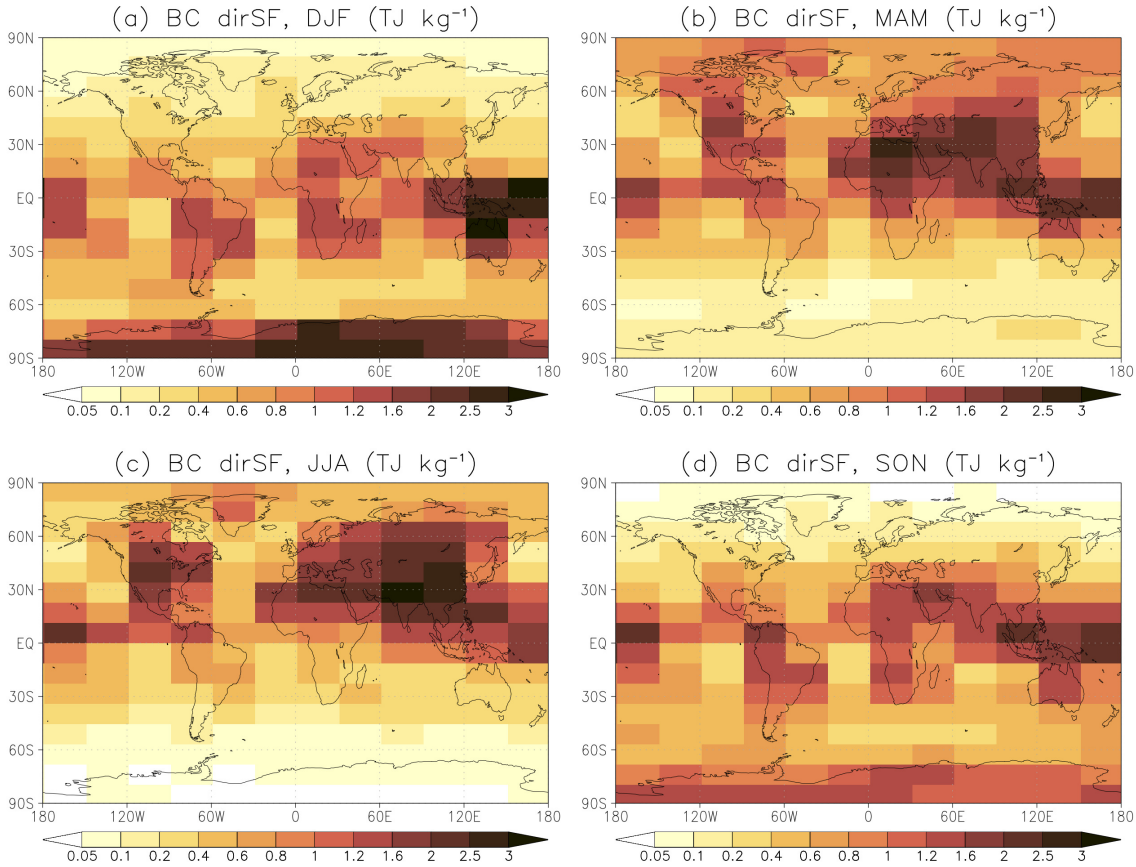

Figure S6. Global-mean values of BC direct specific forcing (in units of TJ kg^{-1}) separately for emissions in 192 lat-lon boxes, for emissions in (a) DJF, (b) MAM, (c) JJA and (d) SON.

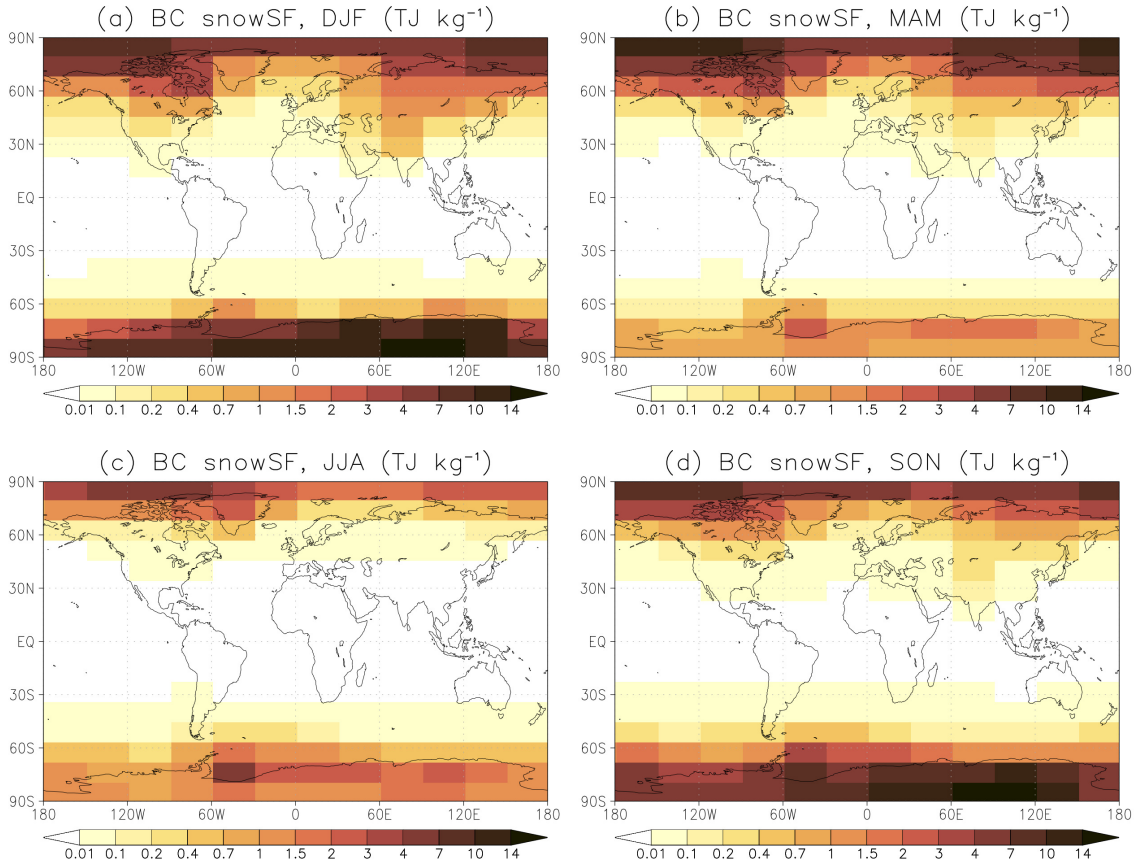

Figure S7. Global-mean values of specific forcing due to BC in snow (in units of $\mathrm{TJ\,kg^{-1}}$) separately for emissions in 192 lat-lon boxes, for emissions in (a) DJF, (b) MAM, (c) JJA and (d) SON.

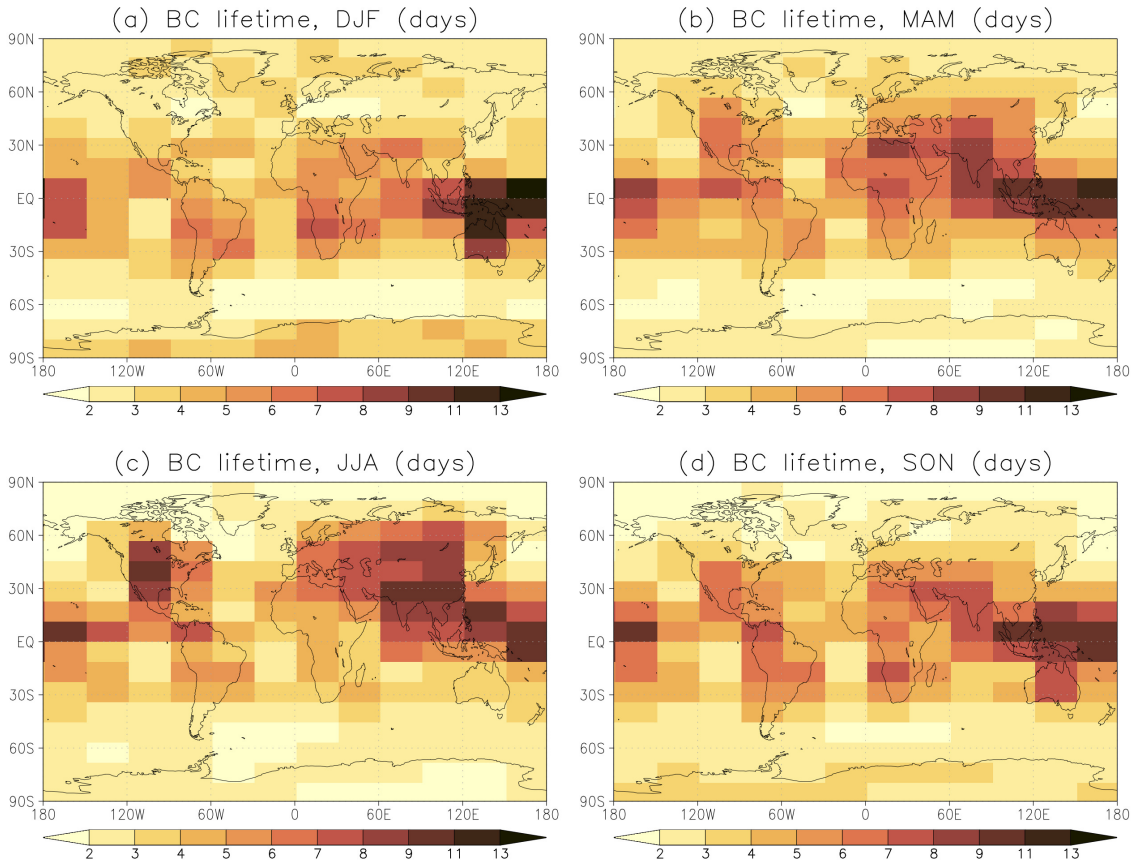

Figure S8. BC lifetime (days) separately for emissions in 192 lat-lon boxes, for emissions in (a) DJF, (b) MAM, (c) JJA and (d) SON.